J Syst Sci Complex (2023) 36: 500–523

Robust Nonsingular Fixed Time Terminal Sliding Mode Control for Atmospheric Pollution Detection Lidar Scanning Mechanism*

KANG Yu · YANG Yuxiao · CHEN Cai · LÜ Wenjun · ZHAO Yunbo

DOI: 10.1007/s11424-023-1011-9
Received: 11 January 2021 / Revised: 10 March 2021

Abstract A robust nonsingular fixed time terminal sliding mode control scheme with a time delay disturbance observer is proposed for atmospheric pollution detection lidar scanning mechanism (APDL-SM) system. Distinguished from the conventional terminal sliding mode control methods, the authors design a novel fixed-time terminal sliding surface, the convergence time of sliding mode phase of which has a constant upper bound that is designable by adjusting only one parameter. Moreover, in order to overcome the problem of unknown upper bound of lumped uncertainty including model uncertainty, friction effect and external disturbances from the port environment, the authors propose a time delay disturbance observer to provide an estimation for the system lumped uncertainty. By using the Lyapunov synthesis, the explicit analysis of the convergence time upper bound are performed. Finally, simulation studies are conducted on the APDL-SM system to show the fast convergence rate and strong robustness of the proposed control scheme.

Keywords Atmospheric pollution detection lidar, fixed time terminal sliding mode, time delay disturbance observer, tracking control.

KANG Yu (Corresponding author)
Department of Automation, University of Science and Technology of China, Hefei 230027*, China; Institute of Advanced Technology, University of Science and Technology of China, Hefei* 230027*, China; State Key Laboratory of Fire Science, University of Science and Technology of China, Hefei* 230027*, China.*
Email: kangduyu@ustc.edu.cn.
YANG Yuxiao · CHEN Cai · LÜ Wenjun · ZHAO Yunbo
Department of Automation, University of Science and Technology of China, Hefei 230027*, China.*
Email: yyx531@mail.ustc.edu.cn; cc95@mail.ustc.edu.cn; wlv@ustc.edu.cn; ybzhao@ieee.org.
*This research was supported by the National Key Research and Development Project of China under Grant Nos. 2018AAA0100800 and 2018YFE0106800, the National Natural Science Foundation of China under Grant Nos. 61903353, 61725304, and 1761673361, Major Science and Technology Project of Anhui Province under Grant No. 912198698036, SINOPEC Programmes for Science and Technology Development under Grant No. PE19008-8, and the Fundamental Research Funds for the Central Universities under Grant No. WK2100000013.
◇ *This paper was recommended for publication by Editor LI Hongyi.*

1 Introduction

Emissions from ships have been recognized as a significant contributor to the atmospheric environment in coastal areas[1, 2]. Exhaust pollutants such as SO_2, NO_x, particulates and carbonaceous compounds would adversely impact regional air quality, global climate and human health[3–5]. With the rapid development of the maritime industry, the impact of exhaust pollutants from ships on air quality could become more serious in the near future[6, 7]. Atmospheric pollution detection lidar (APDL), which is developed based on the differential absorption laser radar technology, could provide an accurate and fast directional monitoring for atmospheric pollution via a long distance. With the assistance of APDL-SM (i.e., the scanning mechanism of APDL), we can scan the atmospheric area over the ship nozzle and then obtain the thermal map of the exhaust plume. Therefore, in order to track the long-range and small-area targets (i.e., nozzles), the control problem of the azimuth and pitch angle of the APDL-SM arises.

The main difficulty is trajectory tracking control with high accuracy and fast response under the issues of high nonlinearity, coupling dynamics, modeling uncertainties, and external disturbances effect. APDL-SM is a typical machinery with two rotational degrees of freedom, the control schemes of which have been investigated intensively, such as event-triggered control[8, 9], adaptive control[10], neural network methods[8, 11], fuzzy logic control[12–14], and sliding mode control (SMC)[15–27]. Adaptive event-triggered neural control problem for nonaffine pure-feedback nonlin-ear multiagent systems with dynamic disturbance, unmodeleddynamics, and dead-zone input was investigated in [8] by using radial basis function neural networks. To solve the leader-following consensus problem for a class of strict-feedback multiagent systems with unknown disturbances and input saturation under a directed topology, a distributed event-triggered control approach based on disturbance observer was proposed in [9]. For robot finger dynamics, [10] proposed a novel design method for adaptive tracking control. Han, et al.[12] presented a funnel dynamic surface control combined with fuzzy echo state networks for the prescribed tracking performance of a strict feedback multi-input-multi-output nonlinear dynamic system.

Among the aforementioned control methods, SMC has attracted significant attention due to its excellent properties such as strong robustness against parameter changes, model uncertainties, and good rejection of external disturbances[17–20, 22]. In [18], a curved path following control algorithm combining sliding mode control (SMC) with the vector field (VF) strategy for miniature unmanned aerial vehicles is developed. [20] proposed three kinds of sliding mode controllers to solve the problem of multi-agent formation control. Gan, et al.[22] proposed a sliding mode control with perturbation estimation coupled with an inverse hysteresis compensator for the motion tracking control of a microposition system with piezoelectric actuation. However, conventional SMC laws are discontinuous and the high-frequency control switching may cause the well-known chattering phenomenon[23, 24]. A robust guidance law based on sliding mode control is formulated in [23], in which the boundary of target maneuver is needed and the chattering phenomenon inevitably exists. In addition, conventional SMC can only guarantee the asymptotic convergence of states, system's states cannot converge to zero in finite time.

To overcome this problem, terminal sliding mode control (TSMC) approach was designed to achieve the finite-time convergence of system dynamics[25]. An adaptive sliding mode control was proposed in [21] such that the sliding surface in the state-estimation space can be reached in a finite time. [28–30] applied non-linear switching manifolds to achieve a fast or finite-time convergence property without imposing strong control force and obtain a finite-time mechanism.

The terminal sliding surface was a nonlinear function of the tracking error and its derivatives, on which the finite-time convergence could be accomplished. Additionally, to eliminate the singularity and accelerate the speed of convergence of TSMC, the nonsingular terminal sliding mode control (NTSMC) and fast nonsingular terminal sliding mode control (FNTSMC) were proposed and achieved successful applications[31–33]. The inherent dynamic properties of the fast terminal sliding modes were explored, and conditions to ensure its applicability for control designs were obtained in [31]. [32] studied fault-tolerant control designs based on nonsingular terminal sliding-mode control and nonsingular fast terminal sliding-mode control, such that the system states reach the control objective point in a finite amount of time. Zheng, et al.[33] proposed a robust motion control method for a linear motor positoner by using fast nonsingular terminal sliding mode control (FNTSMC). Compared with the conventional nonsingular terminal sliding mode control, the FNTSMC can guarantee a faster convergence rate of the tracking error in the presence of system uncertainties which include payload variations, friction, external disturbances, and measurement noises. However, these finite time control methods have a common weakness that the convergence time is affected by the initial state, which means that the control performance of the system might be weakened greatly if the initial state is far away from the sliding surface. Therefore, different from the finite time control methods, the fixed-time control method can guarantee that the convergence time is uniformly bounded by a constant independent of the initial states. [34] modified the second order sliding mode control algorithms by providing global finite-time stability of the closed-loop system, and allowed to adjust a guaranteed settling time independently on initial conditions, which achieved fixed-time stability.

However, there are few results in the machinery tracking control by fixed-time control methods. Meanwhile, considering the uncertainty existing in the system, many studies have used the adaptive control method to approximate the uncertainty. For a class of output feedback nonlinear systems with unmodeled dynamics and output constraint, [35] proposed two dynamic surface control design approaches to solve the adaptive control problem. To design control which renders approximate constraint following, adaptive laws are constructed in [36]. The controls are then based on the adaptive parameters. [37] proposed an integral sliding mode for trajectory tracking control of robotic manipulators by combining integral sliding mode control and adaptive twisting control algorithm. However, the adaptive control usually needs a long time to stabilize, which might cause the divergence and collapse of the system when applied to the actual APDL-SM system.

As one of the well-known practical nonlinear control strategies for uncertainties, time delay control (TDC) employs a time-delayed estimation (TDE) technique to eliminate the unmodeled dynamics, intractable nonlinearity, and external disturbances. [38] studied the the robustness

problem in time-delay control (TDC) for robot manipulators by enhancing the TDC with a compensator based on internal model control (IMC). A time delay estimation based on general framework for trajectory tracking control of robot manipulators is presented in [39]. The controller consists of three elements: A time-delay-estimation element, an injecting element that endows desired error dynamics, and a correcting element. However, in the conventional TDC, the velocity and acceleration signals are calculated by backward differentiator technique, which achieves a lower estimation accuracy due to differentiating the measured position signals[40–42]. To deal with this problem, Van, et al.[43] and Brahmi, et al.[44] used second-order exact differentiation (SOED) to estimate the velocity and acceleration; however, the SOED can only achieve finite time error convergence, which means that the estimation time of system states rely on the initial states. When the initial states of estimation error are far from the original point, the estimation time increases and consequently the tracking performance deteriorates.

In actual application scenarios, APDL-SM is desired to track the chimney of the target ship for exhaust monitoring as quickly as possible and unacted on uncertain factors, such as the model uncertainties, wind speed, wind direction, atmospheric state and other environmental factors. Motivated by actual demands and the attractive attributes of NTSMC, fixed-time control and TDE, a normal control scheme is designed. In this paper, the following design difficulties need to be solved: (i) How to design a drastically novel terminal sliding surface with respect to previous proposals available in the literature, and a reaching law to make the upper bound of the settling time of both reaching phase and sliding mode phase is available, and is independent of the initial state. (ii) How to design the control law to settle the singularity issue arising from the drastically novel terminal sliding surface, and guarantee the control input is nonsingular. (iii) How to design a disturbance observer to estimate and compensate the lumped uncertainty, including model uncertainties, friction effect and external disturbances from the port environment, without the upper bound of lumped uncertainty. A robust nonsingular fixed time terminal sliding mode (RNFTTSM) control scheme with time delay disturbance observer (TDDO) is proposed for the control of APDL-SM. The contributions are threefold:

1) We develop a novel fixed time terminal sliding surface (FTTSS) that the convergence time of sliding mode phase has a constant upper bound. The constant upper bound can be designed by adjusting only one parameter.

2) We propose a new nonsingular fixed time terminal sliding mode (NFTTSM) controller by combining the fixed-time approach law and the proposed FTTSS. The settling time function is upper bounded by a priori value that dose not rely on the system initial state but only on the design parameters. This property implies that the convergence time can be guaranteed in a prescribed manner.

3) We design a novel robust nonsingular fixed time terminal sliding mode (RNFTTSM) control scheme to improve the robustness of system by introducing a designed TDDO. The TDDO could estimate the lumped uncertainty of the system rapidly and accurately.

The rest of the paper is structured as follows: Section 2 provides the modeling process

of APDL-SM and the problem formulation. The notations and preliminaries in this paper are given in Section 3. Section 4 contains the main results, which includes the design of FTTSS, NFTTSM, and RNFTTSM control scheme and the corresponding stability analysis. The simulation results to verify the proposed methods are presented in Section 5. Finally, Section 6 concludes this paper.

2 System Modelling and Problem Formulation

In this section, we derive the kinematic model and dynamic model of APDL-SM at first, and then describe the problem studied in this work mathematically.

2.1 APDL-SM Modeling

As a controlled object in control system, APDL-SM can be divided into three parts in the mechanical structure: Chassis (CAS), azimuth rotating part (ARP) , and pitch rotating part (PRP), which are represented by B_0, B_1, B_2, respectively. The structure diagram of APDL-SM is shown in Figure 1.

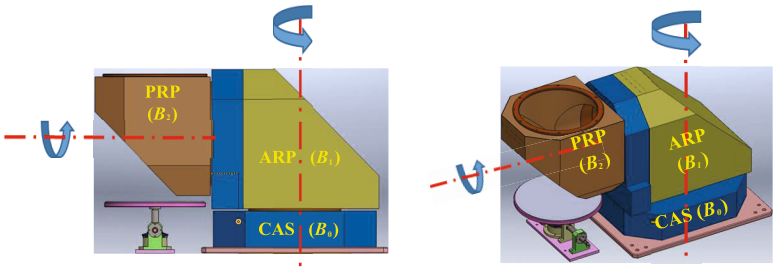

(a) (b)

Figure 1 APDL-SM consists of three parts: CAS (chassis of APDL-SM), ARP (azimuth rotating part), and PRP (pitch rotating part). They are represented by B_0, B_1, B_2, respectively

According to the Denavit-Hartenberg Convention, we establish a link frame for APDL-SM, then carry out the kinematic and the dynamic modelling, which are derived as follows.

2.1.1 Kinematics Modeling

Considering the mechanical structure of the APDL-SM, it can be schematically represented from a mechanical viewpoint as a kinematic chain of two rigid bodies (links) connected by two revolute joints, as shown in Figure 2.

The center of CAS and the central point of the outlet are considered to be the base and end-effector of the kinematic chain, respectively. The joint connecting B_0, and B_1 is considered as *Revolute Jiont* 1. The joint connecting B_1 and B_2 is considered as *Revolute Jiont* 2 which is located at the intersection of the two rotation axes of B_1 and B_2 in the actual mechanism.

According to the Denavit-Hartenberg Convention, the link frame for APDL-SM is established as shown in Figure 3. The origin of *Frame* 0 coincides with *Revolute Jiont* 1. Analogously, the origin of *Frame* 1 locates at the intersection between z_0 and z_1. *Frame* 2 denotes the end-effector frame. $O_{2'}$ denotes the intersection between y_2 and z_1.

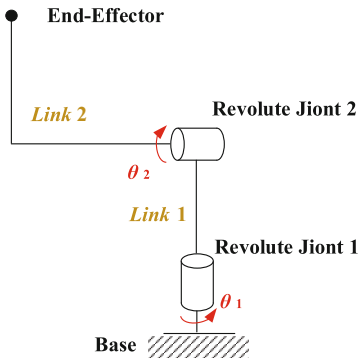

Figure 2 Kinematic Chain

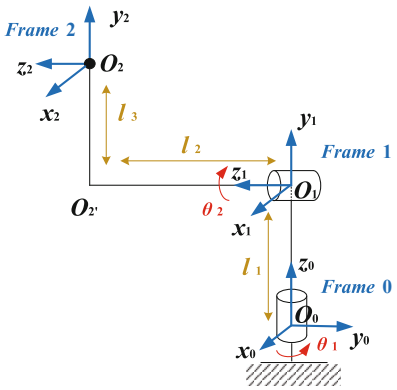

Figure 3 Link frame

On this basis, the Denavit-Hartenberg parameters are specified in Table 1.

Table 1 DH parameters for APDL-SM

Link	a_i	α_i	d_i	θ_i
1	0	$\frac{\pi}{2}$	l_1	θ_1
2	l_3	0	l_2	θ_2

The homogeneous transformation matrices are computed by

$$A_0^1 = A_0^1(\theta_1) = \begin{bmatrix} c_1 & 0 & s_1 & 0 \\ s_1 & 0 & -c_1 & 0 \\ 0 & 1 & 0 & l_1 \\ 0 & 0 & 0 & 1 \end{bmatrix}, \quad A_1^2 = A_1^2(\theta_2) = \begin{bmatrix} c_2 & -s_2 & 0 & l_3 c_2 \\ s_2 & c_2 & 0 & l_3 s_2 \\ 0 & 0 & 1 & l_2 \\ 0 & 0 & 0 & 1 \end{bmatrix}, \tag{2.1}$$

where c_i denotes $\cos\theta_i$, s_i denotes $\sin\theta_i$, and l_1, l_2, l_3 denote the distances between O_0 and O_1, O_1 and $O_{2'}$, $O_{2'}$ and O_2, respectively.

Then the direct kinematics describing the position and orientation of $Frame$ 2 with respect to $Frame$ 0 is given by

$$T_0^2 = A_0^1 \cdot A_1^2 = \begin{bmatrix} c_1c_2 & -c_1s_2 & s_1 & l_3c_1c_2 + l_2s_1 \\ s_1c_2 & -s_1s_2 & -c_1 & l_3s_1c_2 - l_2c_1 \\ s_2 & c_2 & 0 & l_3s_2 + l_1 \\ 0 & 0 & 0 & 1 \end{bmatrix}. \tag{2.2}$$

2.1.2 Dynamic Modeling

For dynamic modeling of APDL-SM with n degrees of freedom ($n = 2$), two methods exist: The Euler-Lagrange and the Newton-Euler method. The former approach is energy-based, while the latter analyzes the forces between each of the links in a recursive manner. Considering the non-uniform and asymmetric properties of the mechanical structure of APDL-SM, the potential

energy changes over the elevation angle during the scanning movement, so the Newton-Euler method is employed.

For the *augmented Link i* (i.e., *Link i* plus *Joint i*) of the kinematic chain (Figure 2) and its center of mass C_i, the modeling procedure consists of two recursions: a forward recursion and a backward recursion[45]. Some symbols used in the procedure are given in Table 2.

Table 2 Symbols in dynamic modeling for *Link i*

Symbol	Description
m_i	mass of *augmented Link i*
I_i^i	inertia tensor of *augmented Link i* with reference to *Frame i*
$\boldsymbol{r}_{i-1,i}^i$	vector from origin of *Frame* $(i-1)$ to origin of *Frame i* with reference to *Frame i*
$\boldsymbol{r}_{i,C_i}^i$	vector from origin of *Frame i* to centre of mass C_i with reference to *Frame i*
$\boldsymbol{\omega}_i^i$	angular velocity of *augmented Link i* with reference to *Frame i*
$\dot{\boldsymbol{\omega}}_i^i$	angular acceleration of *augmented Link i* with reference to *Frame i*
$\boldsymbol{v}_i^i$	linear velocity of origin of *Frame i* with reference to *Frame i*
$\dot{\boldsymbol{v}}_i^i$	linear acceleration of origin of *Frame i* with reference to *Frame i*
$\boldsymbol{v}_{C_i}^i$	linear velocity of centre of mass C_i with reference to *Frame i*
$\dot{\boldsymbol{v}}_{C_i}^i$	linear acceleration of centre of mass C_i with reference to *Frame i*
$\boldsymbol{f}_i^i$	force exerted by *Link* $(i-1)$ on *Link i* with reference to *Frame i*
$\boldsymbol{\rho}_i^i$	moment exerted by *Link* $(i-1)$ on *Link i* with reference to *Frame i*
τ_i	the moment resulting at the *RevoluteJoint i*

For the forward recursion, link and rotor velocities and accelerations can be computed recursively starting from the velocity and acceleration of the base link by using (2.3), (2.4), (2.5), and (2.6), with known initial conditions $\boldsymbol{\omega}_0^0 = \dot{\boldsymbol{\omega}}_0^0 = [0 \quad 0 \quad 0]^{\mathrm{T}}$,

$$\boldsymbol{\omega}_i^i = \boldsymbol{R}_{i-1}^{i\,\mathrm{T}}(\boldsymbol{\omega}_{i-1}^{i-1} + \dot{\theta}_i \boldsymbol{z}_0), \tag{2.3}$$

$$\dot{\boldsymbol{\omega}}_i^i = \boldsymbol{R}_{i-1}^{i\,\mathrm{T}}(\dot{\boldsymbol{\omega}}_{i-1}^{i-1} + \ddot{\theta}_i \boldsymbol{z}_0 + \ddot{\theta}_i \boldsymbol{\omega}_{i-1}^{i-1} \times \boldsymbol{z}_0), \tag{2.4}$$

$$\dot{\boldsymbol{v}}_i^i = \boldsymbol{R}_{i-1}^{i\,\mathrm{T}} \dot{\boldsymbol{v}}_{i-1}^{i-1} + \dot{\boldsymbol{\omega}}_i^i \times \boldsymbol{r}_{i-1,i}^i + \boldsymbol{\omega}_i^i \times (\boldsymbol{\omega}_i^i \times \boldsymbol{r}_{i-1,i}^i), \tag{2.5}$$

$$\dot{\boldsymbol{v}}_{C_i}^i = \dot{\boldsymbol{v}}_i^i + \dot{\boldsymbol{\omega}}_i^i \times \boldsymbol{r}_{i,C_i}^i + \boldsymbol{\omega}_i^i \times (\boldsymbol{\omega}_i^i \times \boldsymbol{r}_{i,C_i}^i), \tag{2.6}$$

where $\boldsymbol{z}_0$ is the unit vector of the rotational axis of revolute joint, i.e., $\boldsymbol{z}_0 = [0 \quad 0 \quad 1]^{\mathrm{T}}$, $\boldsymbol{R}_{i-1}^i$ is the rotation matrix from *Frame* $(i-1)$ into *Frame* i, which can be calculated based on Denavit-Hartenberg parameters:

$$\boldsymbol{R}_0^1 = \begin{bmatrix} c_1 & 0 & s_1 \\ s_1 & 0 & -c_1 \\ 0 & 1 & 0 \end{bmatrix}, \quad \boldsymbol{R}_1^2 = \begin{bmatrix} c_2 & -s_2 & 0 \\ s_2 & c_2 & 0 \\ 0 & 0 & 1 \end{bmatrix}.$$

Having computed the velocities and accelerations with the forward recursion from the base link to the end-effector, the Newton-Euler equations can be utilized to find the forces and moments acting on each link in a backward recursion as (2.7), (2.8), (2.9), starting from the force and moment applied to the end-effector, i.e., $\boldsymbol{f}_{n+1}^{n+1} = \boldsymbol{\rho}_{n+1}^{n+1} = [0 \quad 0 \quad 0]^{\mathrm{T}}$ for $n = 2$.

$$\boldsymbol{f}_i^i = \boldsymbol{R}_i^{i+1}\boldsymbol{f}_{i+1}^{i+1} + m_i\,\dot{\boldsymbol{v}}_{C_i}^{\,i}, \tag{2.7}$$

$$\boldsymbol{\rho}_i^i = -\boldsymbol{f}_i^i \times (\boldsymbol{r}_{i-1,i}^i + \boldsymbol{r}_{i,C_i}^i) + \boldsymbol{R}_i^{i+1}\boldsymbol{\rho}_{i+1}^{i+1} + \boldsymbol{R}_i^{i+1}\boldsymbol{f}_{i+1}^{i+1} \times \boldsymbol{r}_{i,C_i}^i + I_i^{\,i}\dot{\boldsymbol{\omega}}_i^{\,i} + \boldsymbol{\omega}_i^i \times (I_i^i\,\boldsymbol{\omega}_i^i), \tag{2.8}$$

$$\tau_i = \boldsymbol{\rho}_i^{i\mathrm{T}}\,\boldsymbol{R}_{i-1}^{i\ \mathrm{T}}\boldsymbol{z}_0. \tag{2.9}$$

After the above calculations, the dynamic model of APDL-SM is established as follows:

$$M(\theta)\,\ddot{\theta} + C(\theta,\dot{\theta})\,\dot{\theta} + G(\theta) = \tau + \tau_d, \tag{2.10}$$

in which vectors θ, $\dot{\theta}$, $\ddot{\theta} \in \mathbb{R}^2$, $\theta = [\theta_1, \theta_2]^{\mathrm{T}}$ denotes the joint positions, velocities, and accelerations of APDL-SM, respectively. $M(\theta) \in \mathbb{R}^{2\times 2}$ is a positive definite inertia matrix, $C(\theta,\dot{\theta}) \in \mathbb{R}^{2\times 2}$ is the centripetal Coriolis matrix, $G(\theta) \in \mathbb{R}^2$ is the gravitational vector, $\tau = [\tau_1, \tau_2]^{\mathrm{T}} \in \mathbb{R}^2$ is the joint torque input vector generated by the electrical motors connected to the CAS and ARP of APDL-SM, and τ_d is the external disturbance torque vector.

The parameters of APDL-SM are given as follows: $m_1 = 100$ kg, $m_2 = 46.5$ kg, $\boldsymbol{r}_{0,1}^1 = [0\ ,\ 0.18\ ,\ 0]^{\mathrm{T}}$, $\boldsymbol{r}_{1,2}^2 = [0\,,\,0.18\,,\,0.4]^{\mathrm{T}}$, $\boldsymbol{r}_{1,C_1}^{\,1} = [0\,,\,0.16\,,\,0]^{\mathrm{T}}$, $\boldsymbol{r}_{2,C_2}^{\,2} = [0\,,\,-0.14\,,\,0]^{\mathrm{T}}$. The inertia tensors of *augmented Link* 1 and *augmented Link* 2 are

$$I_1^{\,1} = \begin{bmatrix} 5 & 0 & 0 \\ 0 & 5 & -1.2 \\ 0 & -1.2 & 3.2 \end{bmatrix}, \quad I_2^{\,2} = \begin{bmatrix} 2 & 0 & 0 \\ 0 & 1.3 & 0.2 \\ 0 & 0.2 & 2 \end{bmatrix}.$$

Therefore, three nominal matrices in (2.10) are presented as

$$M_0(\theta) = \begin{bmatrix} 9.51\sin^2\theta_2 + 8.74\cos^2\theta_2 + 5 & -0.544\cos\theta_2 \\ -0.544\cos\theta_2 & 2.07 \end{bmatrix}, \tag{2.11}$$

$$C_0(\theta,\dot{\theta}) = \begin{bmatrix} 1.55\sin\theta_2\cos\theta_2\cdot\dot{\theta}_2 & 0.54\sin\theta_2\cdot\dot{\theta}_2 \\ -0.77\sin\theta_2 cos\theta_2\cdot\dot{\theta}_1 & 0 \end{bmatrix}, \tag{2.12}$$

$$G_0(\theta) = \begin{bmatrix} 0 \\ -18.23\sin\theta_2 \end{bmatrix}. \tag{2.13}$$

2.2 Problem Formulation

Considering the modeling uncertainties caused by the asymmetric structural characteristics of APDL-SM, the dynamic equation (2.10) of APDL-SM in the joint space can be expressed as

$$M_0(\theta)\,\ddot{\theta} + C_0(\theta,\dot{\theta})\,\dot{\theta} + G_0(\theta) = \tau + F_d(\theta,\dot{\theta},\ddot{\theta}), \tag{2.14}$$

where $M_0(\theta)$, $C_0(\theta,\dot{\theta})$, $G_0(\theta)$ denote the nominal values, and $F_d(\theta,\dot{\theta},\ddot{\theta}) = \tau_d - \Delta M(\theta)\ddot{\theta} - \Delta C(\theta,\dot{\theta})\dot{\theta} - \Delta G(\theta)$ is the lumped disturbance. $\Delta M(\theta), \Delta C(\theta,\dot{\theta}), \Delta G(\theta)$ stand for the system perturbations, and $\tau_d \in \mathbb{R}^2$ is external disturbances vectors.

The following assumptions are considered for APDL-SM.

Proposition 1 (see [46]) *The inertia matrix $M_0(\theta)$ is positive-definite symmetrical and bounded such that:*

$$\lambda_{\min}(M_0)\, I_{2\times 2} \le M_0(\theta) \le \lambda_{\max}(M_0)\, I_{2\times 2},$$

where $\lambda_{\min}(M_0)$ and $\lambda_{\max}(M_0)$ are the minimum and maximum eigenvalues of the known inertia matrix $M_0(\theta)$ respectively, and $I_{2\times 2}$ is a 2×2 identity matrix.

Proposition 2 *The matrix $\dot{M}_0(\theta) - 2C_0(\theta,\dot{\theta})$ is skew symmetric.*

Let $\theta_d(t) \in \mathbb{R}^2$ be the desired positon azimuth and pitch of the APDL-SM, then the tracking error can be denoted as $\boldsymbol{e}(t) = [e_1(t), e_2(t)]^{\mathrm{T}} \in \mathbb{R}^{2\times 2}$, $\boldsymbol{e}_1(t) = \theta(t) - \theta_d(t)$, and $\boldsymbol{e}_2(t) = \dot{\theta}(t) - \dot{\theta}_d(t)$. The control objective of this paper is to design a nonsingular SMC for APDL-SM, such that the tracking error $\boldsymbol{e}(t)$ can converge to zero within a fixed amount of time, even if APDL-SM is under the effect of unmodeled dynamics, friction vibration and external disturbances:

$$\lim_{t\to t_c} \|\boldsymbol{e}(t)\| = 0, \tag{2.15}$$

where $t_c = t_r + t_s$ is the total settling time of reaching phase and sliding mode phase, and it is available and independent of the initial state.

To solve these problems, let $x_1(t) = \theta(t) \in \mathbb{R}^2$, $x_2(t) = \dot{\theta}(t) \in \mathbb{R}^2$, $x(t) = [x_1(t), x_2(t)]^{\mathrm{T}} \in \mathbb{R}^{2\times 2}$, based on the state space form in [43], APDL-SM dynamic equation (2.14) can be rewritten as:

$$\begin{aligned} \dot{x}_1(t) &= x_2(t), \\ \dot{x}_2(t) &= f(t,x) + g(t,x)\, u + d(t,x), \end{aligned} \tag{2.16}$$

where $f(t,x) = {M_0}^{-1}(x_1)\big[- C_0(x_1,x_2)\, x_2 - G_0(x_1)\big]$, $g(t,x) = {M_0}^{-1}(x_1)$, and $d(t,x) = {M_0}^{-1}(x_1) \cdot F_d(x_1,x_2,\dot{x}_2)$. $u = \tau$ is the control input. The following assumptions are imposed on system.

Assumption 1 The desired trajectory $\theta_d(t)$ and its first and second-order derivative are known and bounded.

Assumption 2 The lumped uncertainty term $d(t,x)$ is bounded by a known function:

$$\| d(t,x) \| \le \Xi(x), \quad \forall(t) \ge 0, \quad \forall(x) \in \mathbb{R}^{2\times 2}. \tag{2.17}$$

Assumption 3 The angular position $\theta(t)$, angular velocity $\dot{\theta}(t)$ and angular acceleration $\ddot{\theta}(t)$ are available.

3 Notations and Preliminaries

3.1 Notations

$\mathbb{R}$ denotes the set of real numbers. $\mathbb{R}^+$ denotes the set of positive real numbers. $\mathbb{R}^n$ represents the set of n column vectors. $\mathbb{R}^{n\times n}$ represents the set of $n\times n$ matrices.

As for a vector $a=[a_1,a_2,\cdots,a_n]^{\mathrm{T}}\in\mathbb{R}^n$, define the absolute value of a as $|a|=\big[|a_1|,|a_2|,\cdots,|a_n|\big]^{\mathrm{T}}\in\mathbb{R}^n$, where $|\cdot|$ denotes the absolute value of a scalar. The norm of vector a is defined as the Euclidean norm, i.e., $\|a\|=\sqrt{a^{\mathrm{T}}a}$. For the signum function $\mathrm{sgn}(\cdot)$ and a constant γ, define:

$a^{\gamma}=\big[{a_1}^{\gamma},{a_2}^{\gamma},\cdots,{a_n}^{\gamma}\big]^{\mathrm{T}}\in\mathbb{R}^n$

$\mathrm{sgn}(a)=\big[\mathrm{sgn}(a_1),\mathrm{sgn}(a_2),\cdots,\mathrm{sgn}(a_n)\big]^{\mathrm{T}}\in\mathbb{R}^n$,

$\lfloor a\rceil^{\gamma}:=\big[|a_1|^{\gamma}\mathrm{sgn}(a_1),|a_2|^{\gamma}\mathrm{sgn}(a_2),\cdots,|a_n|^{\gamma}\mathrm{sgn}(a_n)\big]^{\mathrm{T}}\in\mathbb{R}^n$,

$\lceil a\rfloor^{\gamma}:=\mathrm{diag}\Big(|a_1|^{\gamma}\mathrm{sgn}(a_1),|a_2|^{\gamma}\mathrm{sgn}(a_2),\cdots,|a_n|^{\gamma}\mathrm{sgn}(a_n)\Big)\in\mathbb{R}^{n\times n}$,

$(a+1)^{\gamma}:=\big[(a_1+1)^{\gamma},(a_2+1)^{\gamma},\cdots,(a_n+1)^{\gamma}\big]^{\mathrm{T}}\in\mathbb{R}^n$,

$\langle a+1\rangle^{\gamma}:=\mathrm{diag}\Big((|a_1|+1)^{\gamma},(|a_2|+1)^{\gamma},\cdots,(|a_n|+1)^{\gamma}\Big)\in\mathbb{R}^{n\times n}$.

As for a matrix $X\in\mathbb{R}^{m\times n}$, $\|X\|$ represents the Euclidean norm, $X^{\sharp}$ denotes the column vector of the sum of the absolute values of the elements in each row, i.e.,

$$X^{\sharp}:=\left[\sum_{j=1}^{n}|x_{1j}|,\ \sum_{j=1}^{n}|x_{2j}|,\cdots,\ \sum_{j=1}^{n}|x_{mj}|\right]^{\mathrm{T}}\in\mathbb{R}^n.$$

3.2 Preliminaries

Consider the following differential equation system:

$$\dot{x}(t)=F(x(t)),\quad x(0)=x_0, \tag{3.1}$$

where $x\in\mathbb{R}^N$, $F(x):\mathbb{R}_+\times\mathbb{R}^N\to\mathbb{R}^N$ is a nonlinear function. Suppose that the origin is an equilibrium point of (3.1).

Definition 1 (see [47]) The origin of the system (3.1) is a finite-time stable equilibrium if the origin is Lyapunov stable and there exists a function $T:\mathbb{R}^N\to\mathbb{R}_+$, called the settling time function, such that for every $x_0\in\mathbb{R}^N$. The solution $x(t,x_0)$ of the system (3.1) is defined on $[0,T(x_0))$, with $x(t,x_0)\in\mathbb{R}^N$ for all $t\in[0,T(x_0))$, and $\lim_{t\to T_{x_0}}x(t,x_0)=0$.

Definition 2 (see [47]) The origin of (3.1) is said to be a fixed-time stable equilibrium point if it is globally finite-time stable with bounded settling time $T(x_0)$, i.e., $\exists\ T_{\max}>0$ such that $T(x_0)<T_{\max}$, $\forall x_0\in\mathbb{R}^N$.

Lemma 1 (see [48]) *Consider a scalar system*

$$\dot{y}=-\alpha\, y^{\frac{m}{n}}-\beta\, y^{\frac{p}{q}},\quad y(0)=y_0, \tag{3.2}$$

where $\alpha>0$, $\beta>0$, and m,n,p,q are positive odd integers satisfying $m>n$ and $p>q$. Then the equilibrium of (3.2) *is fixed-time stable and the settling time T is bounded by*

$$T<T_{\max}\triangleq\frac{1}{\alpha}\,\frac{n}{m-n}+\frac{1}{\beta}\,\frac{q}{q-p}. \tag{3.3}$$

4 Control Scheme Design and Stability Analysis

It consists of two parts: NFTTSM controller and the RNFTTSM control scheme, which combines NFTTSM with a time delay distuebance observer (TDDO). They will be introduced in detail respectively as follows.

4.1 FTTSS

First of all, a new fixed time terminal sliding surface (FTTSS) is designed as:

$$\sigma(e) = e_2 + 2\beta \lceil e_1 \rfloor^{\frac{1}{2}} (|e_1| + 1)^{\frac{3}{2}}, \tag{4.1}$$

where $\beta = \mathrm{diag}(\beta_1, \beta_2)$ is a positive definite matrix.

Theorem 1 *Consider the tracking error dynamic system* (2.14) *with our proposed FTTSS* (4.1) *satisfying* $\sigma = 0$. *Then* $e_1 = 0$ *and* $e_2 = 0$ *can be reached in a fixed time* t_s, *whose upper bound can be estimated as*

$$t_s \le T_s = (\beta^{-1})^{\sharp}. \tag{4.2}$$

Proof Once a sliding motion is established on the surface $\sigma = 0$, the dynamics of the variable $e_1(t)$ are governed by

$$\dot{e}_1 = -2\beta \lceil e_1 \rfloor^{\frac{1}{2}} (|e_1| + 1)^{\frac{3}{2}}. \tag{4.3}$$

Considering $\dot{e}_1 = \frac{de_1}{dt}$, Equation (4.3) can be written as

$$\frac{de_1}{dt} = -2\beta \lceil e_1 \rfloor^{\frac{1}{2}} (|e_1| + 1)^{\frac{3}{2}}, \tag{4.4}$$

$$-\beta\, dt = \frac{1}{2} \lceil e_1 \rfloor^{-\frac{1}{2}} (|e_1| + 1)^{-\frac{3}{2}}\, de_1. \tag{4.5}$$

To solve the differential equation (4.5), integrate both sides of this equation at first, then (4.5) can be written as

$$\int dt = -(2\beta)^{-1} \int \lceil e_1 \rfloor^{-\frac{1}{2}} (|e_1| + 1)^{-\frac{3}{2}}\, de_1, \tag{4.6}$$

$$t_s - t_0 = -(2\beta)^{-1} \int |e_1|^{-\frac{1}{2}} (|e_1| + 1)^{-\frac{3}{2}}\, d(|e_1|), \tag{4.7}$$

$$t_s = -\beta^{-1} \int (|e_1| + 1)^{-\frac{3}{2}} d(|e_1|^{\frac{1}{2}}). \tag{4.8}$$

Let $|e_1|^{\frac{1}{2}} = \tan z$, then we have

$$z = \arctan(|e_1|^{\frac{1}{2}}), \tag{4.9}$$

$$(|e_1| + 1)^{-\frac{3}{2}} = (\tan^2 z + 1)^{-\frac{3}{2}} = \left(\frac{\sin^2 z}{\cos^2 z} + 1\right)^{-\frac{3}{2}} = \left(\frac{1}{\cos^2 z}\right)^{-\frac{3}{2}} = \cos^3 z. \tag{4.10}$$

Substituting (4.9) into (4.8), the convergence time t_s of sliding mode phase is

$$t_s = -\beta^{-1} \int \cos^3 z \, d(\tan z) \tag{4.11}$$

$$= -\beta^{-1} \int \cos z \, dz \tag{4.12}$$

$$= -\beta^{-1}(\sin z - \sin z_0). \tag{4.13}$$

Considering $z = \arctan(|e_1|^{\frac{1}{2}})$, substitute it into (4.13), then we have

$$t_s = -\beta^{-1}\big[\sin\big(\arctan(|e_1(t_s)|^{\frac{1}{2}})\big) - \sin\big(\arctan(|e_1(t_0=0)|^{\frac{1}{2}})\big)\big]. \tag{4.14}$$

Since the end state of sliding mode phase is $e_1(t_s) = 0$ and $e_1(0)$ represents the initial state, (4.14) can be written as

$$t_s = \beta^{-1} \sin\big(\arctan(|e_1(0)|^{\frac{1}{2}})\big). \tag{4.15}$$

Due to $\sin(\arctan\gamma) = \frac{\gamma}{\sqrt{1+\gamma^2}}$, (4.15) is equal to

$$t_s = \beta^{-1} \, |e_1(0)|^{\frac{1}{2}} \, (|e_1(0)|+1)^{-\frac{1}{2}}. \tag{4.16}$$

Consider that the upper bound of both elements in the vector $|e_1(0)|^{\frac{1}{2}} \, (|e_1(0)|+1)^{-\frac{1}{2}}$ is 1, therefore, once the sliding surface is attained, the states e_1, e_2 can reach the origin within a fixed time with the upper bound T_s:

$$t_s = \beta^{-1} \, |e_1(0)|^{\frac{1}{2}} \, (|e_1(0)|+1)^{-\frac{1}{2}} \leq \beta^{-1} \tag{4.17}$$

$$\Longrightarrow t_s \leq T_s = (\beta^{-1})^{\sharp}. \tag{4.18}$$

Because there are two rotation angles to be controled, each of them can be designed the upper bound of convergence time separately. Therefore, $(\cdot)^{\sharp}$ denotes the column vector of a matrix, which calculates the sum of the absolute values of the elements in each row. ∎

4.2 NFTTSM Controller

Considering Assumption 3 that the angular position $\theta(t)$ and angular velocity $\dot{\theta}(t)$ are both available, we design a controller for the system (2.14) such that the desired trajectory can be reached in fixed time, which means that the total convergence time is independent of initial states.

According to the terminal sliding mode design procedure, the nonsingular fixed time terminal sliding mode controller is designed as

$$u = u_{eq} + u_{re}, \tag{4.19}$$

where u_{eq} is used to control nominal component, and u_{re} is introduced to deal with the uncertainty. u_{eq} can be obtained by solving the equation $\dot{\sigma} = 0$ with $d(t,x) = 0$

$$u_{eq} = -g^{-1}(t,x)\Big[f(t,x) + 4\beta\lceil e_1\rfloor^{\frac{1}{2}}\langle e_1+1\rangle^{\frac{1}{2}}e_2 + \mathrm{sat}\Big(\beta\lceil e_1\rfloor^{-\frac{1}{2}}\langle e_1+1\rangle^{\frac{1}{2}}e_2,\ h\Big)\Big]. \tag{4.20}$$

In (4.20), a saturation function is applied to handle the singularity by limiting the amplitude of singularity term $\lceil e_1 \rfloor^{-\frac{1}{2}}$, and the saturation function can be defined as

$$\mathrm{sat}(x, y) = \begin{cases} x, & \text{if } |x| < y, \\ y \cdot \mathrm{sgn}(x), & \text{if } |x| \geq y. \end{cases} \tag{4.21}$$

To guarantee the fixed-time convergence to the sliding surface, revisit Lemma 1 and then design the reaching law:

$$\dot{\sigma} = -k_1 \, \sigma^{\frac{p}{q}} - k_2 \, \sigma^{\frac{m}{n}} - \Xi(x)\mathrm{sgn}(\sigma), \tag{4.22}$$

where $k_1 = \mathrm{diag}(k_{11},\, k_{12})$, $k_2 = \mathrm{diag}(k_{21},\, k_{22})$ are positive definite matrix, m, n, p, q are positive odd integers satisfying $m > n$ and $p < q$. Therefore, we can obtain u_{re} as

$$u_{re} = -g^{-1}(t, x)\big[k_1 \, \sigma^{\frac{p}{q}} + k_2 \, \sigma^{\frac{m}{n}} + \Xi(x)\mathrm{sgn}(\sigma)\big]. \tag{4.23}$$

Theorem 2 *Considering the dynamic system* (2.16) *satisfying Assumptions* 1, 2, 3*, the sliding mode* σ *and the tracking errors* e_1 *and* e_2 *will converge to the origin within a fixed time via the proposed FTTSS* (4.1) *and NFTTSM controller* (4.19), (4.20), (4.23)*, and the settling time* t_c *is bounded by*

$$t_c \leq T_c = \left(\beta^{-1} + \frac{n}{m-n} {k_1}^{-1} + \frac{q}{q-p} {k_2}^{-1}\right)^{\sharp}. \tag{4.24}$$

Proof Consider the following Lyapunov candidate function as

$$V_1 = \frac{1}{2}\sigma^{\mathrm{T}}\sigma. \tag{4.25}$$

The time derivative of V_1 can be obtained as $\dot{V}_1 = \sigma^{\mathrm{T}}\dot{\sigma}$, and yields

$$\dot{V}_1 = \sigma^{\mathrm{T}}\Big[f(t, x) + g(t, x)\, u + d(t, x) + 4\beta\lceil e_1 \rfloor^{\frac{1}{2}} \langle e_1 + 1\rangle^{\frac{1}{2}} e_2 + \beta\lceil e_1 \rfloor^{-\frac{1}{2}} \langle e_1 + 1\rangle^{\frac{1}{2}} e_2\Big]. \tag{4.26}$$

Substituting the NFTTSM controller (4.19), (4.20), (4.23) into (4.26), we have

$$\begin{aligned} \dot{V}_1 &= -\sigma^{\mathrm{T}}\Big[k_1\sigma^{\frac{p}{q}} + k_2\sigma^{\frac{m}{n}} + \Xi(x)\mathrm{sgn}(\sigma) - d(t, x) + \mathrm{sat}(\Gamma, h) - \Gamma\Big] \\ &= -\sigma^{\mathrm{T}}\Big[k_1\sigma^{\frac{p}{q}} + k_2\sigma^{\frac{m}{n}}\Big] - \sigma^{\mathrm{T}}\Big[\Xi(x)\mathrm{sgn}(\sigma) - d(t, x)\Big] - \sigma^{\mathrm{T}}\Big[\mathrm{sat}(\Gamma, h) - \Gamma\Big] \\ &\leq -\lambda_{\min}(k_1)V^{\frac{p+q}{2q}} - \lambda_{\min}(k_2)V^{\frac{m+n}{2n}} - \|\sigma\|\big[\Xi(x) - \|d(t, e)\|\big] - \|\sigma\|\left[\|\mathrm{sat}(\Gamma, h)\| - \|\Gamma\|\right] \\ &= -\lambda_{\min}(k_1)V^{\frac{p+q}{2q}} - \lambda_{\min}(k_2)V^{\frac{m+n}{2n}} - \|\sigma\| \cdot \mu - \|\sigma\| \cdot \nu, \end{aligned} \tag{4.27}$$

where $\Gamma = \beta\lceil e_1 \rfloor^{-\frac{1}{2}} \langle e_1 + 1\rangle^{\frac{1}{2}} e_2$, $\mu = \Xi(x) - \|d(t, x)\|$, $\nu = \|\mathrm{sat}(\Gamma, h)\| - \|\Gamma\|$, $\lambda_{\min}(k_i)$ denotes the minimum eigenvalue of the positively definite matrix k_i, therefore, we have

$$-\lambda_{\min}(k_1)\, V^{\frac{p+q}{2q}} - \lambda_{\min}(k_2)\, V^{\frac{m+n}{2n}} < 0. \tag{4.28}$$

According to (2.17), one has $\mu = \Xi(x) - \|d(t, x)\| > 0$ so that it yields

$$-\|\sigma\| \cdot \mu < 0. \tag{4.29}$$

To confirm the sign of $-\|\sigma\|\cdot\nu$, define the singularity area Ω as the region where inequality $|\Gamma| \geq h$ holds. The following analysis will be divided into two cases.

For the case of $|\Gamma| < h$, on the basis of (4.21), we have $\mathrm{sat}(\Gamma, h) = \Gamma$, which gives rise to $\nu = \|\mathrm{sat}(\Gamma, h)\| - \|\Gamma\| = 0$, thus $-\|\sigma\|\cdot\nu < 0$. Based on the (4.28) and (4.29), it is concluded that $\dot{V}_1 < 0$, so that it is asymptotically stable.

For the case of $|\Gamma| \geq h$, the tracking error $e_1(t)$ can be obtained by $e_1(t) = e_1(0) + \int_0^t e_2(\tau)d\tau$. If $e_2(t) > 0$ holds, $e_1(t)$ will increase monotonically and leave the singularity area Ω. If e_2 $(t < 0)$ holds, $e_1(t)$ will decrease monotonically and also leave the singularity area. Both situations prove that the system lies in the singularity region transiently. Therefore, the existence of singularity region does not influence the results of the stability analysis.

According to Lemma 1 and the reaching law in (4.22), the system (2.16) reaches the sliding surface within a bounded time, and the bound of convergence time can be estimated by

$$t_r \leq T_r = \left(\frac{n}{m-n}{k_1}^{-1} + \frac{q}{q-p}{k_2}^{-1}\right)^{\sharp}. \tag{4.30}$$

When the system reaches the sliding surface $\sigma = 0$, recalling Theorem 1 yields that the state variable $e_1(t)$ can be stabilized within a finite time bounded by

$$t_s \leq T_s = (\beta^{-1})^{\sharp}. \tag{4.31}$$

When state variable $e_1(t)$ settles down to the origin, the state variable $e_2(t)$ also converges to zero. Consequently, the convergence time for the system (2.16) can be estimated as

$$t_c = t_r + t_s \leq T_r + T_s = \left(\beta^{-1} + \frac{n}{m-n}{k_1}^{-1} + \frac{q}{q-p}{k_2}^{-1}\right)^{\sharp}. \tag{4.32}$$

The proof is completed. ∎

Remark 1 In order to guarantee that $\sigma = 0$ lies outside the singularity area Ω, as pointed out in [47], the parameter h in control law (4.20) can be set to satisfy

$$h > \beta\lceil e_{1\max}\rfloor^{-\frac{1}{2}}\langle e_{1\max}+1\rangle^{\frac{1}{2}} \cdot \left(2\beta\,\lceil e_{1\max}\rfloor^{\frac{1}{2}}(|e_{1\max}|+1)^{\frac{3}{2}}\right) \tag{4.33}$$

$$\Longrightarrow h > 2\beta^2 \cdot \left(|e_{1\max}|+1\right)^2, \tag{4.34}$$

where $e_{1\max}$ denotes the maximum of $|e_1|$.

Remark 2 In the proposed controller (4.19), (4.20), (4.23), the design procedure is based on the assumption that the upper bound function $\Xi(x)$ of the unknown function $d(t, x)$ can be obtained in advance. However, this approach limits its applications because the exact upper bound function is difficult to obtain beforehand in real world. In order to overcome this drawback, a TDDO will be developed in the next section, and the RNFTTSM control scheme is proposed as a result.

4.3 RNFTTSM

In this section, we propose a robust nonsingular fixed time terminal sliding mode (RNFTTSM) contol scheme based on a time delay disturbance observer (TDDO). Another assumption is made as follows.

Assumption 4 The lumped uncertainty term $d(t,x)$ is continuous over time t and continuously differentiable with respect to the time variable, and do not vary largely during a small period T_L of time.

According to the above assumption, the lumped uncertainty term $d(t,x)$ can be considered as a continuous function, and thus the following approximation is satisfied based on TDE technique:

$$d(t,x) \cong d(t-T_L,x). \tag{4.35}$$

Consequently, the estimation of the $d(t,e)$ can be obtained, that is,

$$\widehat{d}(t,x) \triangleq d(t-T_L,x), \tag{4.36}$$

where $\widehat{d}(t,x)$ is the estimation of lumped uncertainty $d(t,x)$ at the time t.

Remark 3 In practice, the smallest achievable T_L is the sampling period in digital implementation. A digital control system behaves reasonably close to the continuous system if the sampling rate is faster than 30 times the system bandwidth[49]. Hence, with a T_L smaller than this level, the continuous lumped uncertainty $d(t,e)$ can be estimated by using the TDE.

From the dynamic system (2.16) and (4.36), the TDDO can be obtained as

$$\widehat{d}(t,x) \triangleq d(t-T_L,x) = \dot{x}_2(t-T_L) - f(t-T_L,x) - \Big(g(t-T_L,x)u\Big) = d_{TDDO}, \tag{4.37}$$

where

$$f(t-T_L,x) = \Big\{{M_0}^{-1}(x_1)\big[-C_0(x_1,x_2)x_2 - G_0(x_1)\big]\Big\}\Big|_{t-T_L}$$

and

$$g(t-T_L,x) = \big\{{M_0}^{-1}(x_1)\big\}\Big|_{t-T_L}.$$

From (4.35), (4.37), the unknown lumped uncertainty function can be described by the proposed TDDO with the observation error δ as

$$d(t,x) = d_{TDDO} + \delta, \tag{4.38}$$

where δ is the observation error. Based on the analyses in [50, 51], the assumption below is reasonable for a sufficiently small T_L.

Assumption 5 There exists a positive constant $\overline{\delta}$ such that $|\delta| \le \overline{\delta}$, and $\overline{\delta}$ is a known upper bound of TDDO error.

From (4.38), the dynamic system described in (2.16) can be rewritten as

$$\begin{aligned} \dot{x}_1(t) &= x_2(t), \\ \dot{x}_2(t) &= f(t,x) + g(t,x)\,u + d_{TDDO} + \delta. \end{aligned} \tag{4.39}$$

For this system, the derivative of the sliding surface σ defined in (4.1) can be rewritten as

$$\begin{aligned}\dot{\sigma} =& f(t,x) + g(t,x)\,u + d_{H\text{-}TDDO} + \delta \\ &+ 4\beta\lceil e_1\rfloor^{\frac{1}{2}}\langle e_1+1\rangle^{\frac{1}{2}}e_2 + \beta\lceil e_1\rfloor^{-\frac{1}{2}}\langle e_1+1\rangle^{\frac{1}{2}}e_2.\end{aligned} \tag{4.40}$$

Then the RNFTTSM control scheme is now designed based on TDDO to accommodate unmodeled dynamics, friction vibration and external disturbances.

$$u = u_{eq} + u_{TDDO} + u_{re}, \tag{4.41}$$

where u_{eq} is designed as the same as (4.20):

$$u_{eq} = -g^{-1}(t,x)\left[f(t,x) + 4\beta\lceil e_1\rfloor^{\frac{1}{2}}\langle e_1+1\rangle^{\frac{1}{2}}e_2 + \mathrm{sat}\Big(\beta\lceil e_1\rfloor^{-\frac{1}{2}}\langle e_1+1\rangle^{\frac{1}{2}}e_2,\ h\Big)\right]. \tag{4.42}$$

The lumped uncertainty compensation term based on TDDO is

$$u_{TDDO} = -g^{-1}(t,x)\ d_{TDDO} \tag{4.43}$$

and u_{re} is designed as

$$u_{re} = -g^{-1}(t,x)\big[k_1\,\sigma^{\frac{p}{q}} + k_2\,\sigma^{\frac{m}{n}} + \overline{\delta}\cdot\mathrm{sgn}(\sigma)\big]. \tag{4.44}$$

The parameters in (4.44) have the same definitions in (4.23). And the stability of the system under the proposed RNFTTSM control scheme in (4.43) is demonstrated as follows.

Theorem 3 *Considering the APDL-SM dynamic system* (4.39) *under Assumption* 1 *to Assumption* 5*, the sliding mode* σ *and the tracking errors* e_1 *and* e_2 *will converge to the origin within a fixed time via the proposed FTTSS* (4.1) *and RNFTTSM control law* (4.41)*,* (4.42)*,* (4.43)*,* (4.44)*.*

Proof Let the Lyapunov candidate function be

$$V_2 = \frac{1}{2}\,\sigma^{\mathrm{T}}\sigma. \tag{4.45}$$

Differentiating V_2 with respect to time and substitute (4.40) into it, we have

$$\begin{aligned}\dot{V}_2 &= \sigma^{\mathrm{T}}\dot{\sigma} \\ &= \sigma^{\mathrm{T}}\Big[f(t,x) + g(t,x)u + (d_{TDDO} + \delta) \\ &\qquad + 4\beta\lceil e_1\rfloor^{\frac{1}{2}}\langle e_1+1\rangle^{\frac{1}{2}}e_2 + \beta\lceil e_1\rfloor^{-\frac{1}{2}}\langle e_1+1\rangle^{\frac{1}{2}}e_2\Big],\end{aligned} \tag{4.46}$$

then, substitute the RNFTTSM control law (4.41) to (4.44) into above, it yields

$$\begin{aligned}\dot{V}_2 &= -\sigma^{\mathrm{T}}\big[\mathrm{sat}(\Gamma,h) - \Gamma + k_1\sigma^{\frac{p}{q}} + k_2\sigma^{\frac{m}{n}} + \overline{\delta}\cdot\mathrm{sgn}(\sigma) - \delta\big] \\ &= -\sigma^{\mathrm{T}}\big[k_1\sigma^{\frac{p}{q}} + k_2\sigma^{\frac{m}{n}}\big] - \sigma^{\mathrm{T}}\big[\overline{\delta}\cdot\mathrm{sgn}(\sigma) - \delta\big] - \sigma^{\mathrm{T}}\Big[\mathrm{sat}(\Gamma,h) - \Gamma\Big] \\ &\le -\lambda_{\min}(k_1)V^{\frac{p+q}{2q}} - \lambda_{\min}(k_2)V^{\frac{m+n}{2n}} - \|\sigma\|\Big[\|\mathrm{sat}(\Gamma,h)\| - \|\Gamma\|\Big] \\ &= -\lambda_{\min}(k_1)V^{\frac{p+q}{2q}} - \lambda_{\min}(k_2)V^{\frac{m+n}{2n}} - \|\sigma\|\cdot\nu,\end{aligned} \tag{4.47}$$

where Γ and ν have the same definations as (4.27).

Based on (4.47) and the proof for Theorem 1, we can verify that the trajectories of (4.1) and the tracking errors e_1 and e_2 will converge to the origin within fixed time without singularity under the control law defined in (4.41) to (4.44). This completes the proof for Theorem 3. ∎

Remark 4 Considering that the proposed control laws (4.23) and (4.44) consist the signum function sgn(·), the chattering is inevasible in the system. However, the chattering amplitude is related to the upper bound of lumped uncertainty or the upper bound of TDDO error. Therefore, the chattering can be reduced to the acceptable limits due to TDDO, and the proposed methods can used in APDL-SM system.

5 Comparative Study and Discussion

To demonstrate the effectiveness of the proposed RNFTTSM control schemes, numerical simulations for the azimuth and pitch angle of the APDL-SM to track a given desired trajectory are carried out under the proposed control scheme.

In this section, NFTTSM (4.19) and the adaptive SOFNTSM controller (see [52]) are considered in simulations for the purpose of comparison to demonstrate the superiority of the RNFFTSM controller (4.41) more clearly.

Rewrite the dynamic equation of APDL-SM (2.14) as follows:

$$M_0(\theta)\,\ddot{\theta} + C_0(\theta,\dot{\theta})\,\dot{\theta} + G_0(\theta) = \tau + F_d(\theta,\dot{\theta},\ddot{\theta}), \tag{5.1}$$

where the three nominal matrices are presented as

$$M_0(\theta) = \begin{bmatrix} 9.51\sin^2\theta_2 + 8.74\cos^2\theta_2 + 5 & -0.544\cos\theta_2 \\ -0.544\cos\theta_2 & 2.07 \end{bmatrix}, \tag{5.2}$$

$$C_0(\theta,\dot{\theta}) = \begin{bmatrix} 1.55\sin\theta_2\cos\theta_2\cdot\dot{\theta}_2 & 0.54\sin\theta_2\cdot\dot{\theta}_2 \\ -0.77\sin\theta_2 cos\theta_2\cdot\dot{\theta}_1 & 0 \end{bmatrix}, \tag{5.3}$$

$$G_0(\theta) = \begin{bmatrix} 0 \\ -18.23\sin\theta_2 \end{bmatrix}. \tag{5.4}$$

The desired trajectory for azimuth and pitch angle of APDL-SM are selected as

$$\theta_d = \begin{bmatrix} 1.45 - 1.4\mathrm{e}^{-t} + 0.6\mathrm{e}^{-4t} \\ 1.25 + \mathrm{e}^{-t} - 0.5\mathrm{e}^{-4t} \end{bmatrix}. \tag{5.5}$$

The unmodeled dynamics including parametric uncertainties is chosen as 0.2 times the normal dynamics, while the external disturbances follows

$$\tau_d = \begin{bmatrix} 2\sin t + 0.5\sin(200\,\pi t) \\ \cos(2t) + 0.5\sin(200\,\pi t) \end{bmatrix}. \tag{5.6}$$

The comparative simulations of RNFTTSMC, NFTTSMC and the adaptive SOFNTSM controller are conducted with the same initial conditions $x(0)^1 = [0.2, 2.1, 0, -0.1]^{\mathrm{T}}$. The parameters of RNFTTSM and NFTTSM controller are selected as $k_1 = 0.5, k_2 = 1, m = 5, n = 3, p = 1, q = 9, \beta_1 = \beta_2 = 8$. Besides, to verify the fixed time convergence of NFTTSMC, another four initial states are considered $x(0)^1 = [0.2, 2.1, 0, -0.1]^{\mathrm{T}}$, $x(0)^2 = [0.8, 3, 0.5, 0.5]^{\mathrm{T}}$, $x(0)^3 = [1.2, 0.2, -0.4, 1.4]^{\mathrm{T}}$, $x(0)^4 = [1.5, 1.3, 0.1, 6]^{\mathrm{T}}$, $x(0)^5 = [-0.4, 2.3, -0.2, -3]^{\mathrm{T}}$. Under the above settings, the angle and angular velocity tracking performances of ARP and PRP under three controller are depicted from Figures 4–7. Each and every component in contributions are illustrated as follows with a clear explanation about the simulation results with respect to each figure.

1) Tracking performance of RNFTTSM control scheme.

By comparing the responses under the RNFTTSM controller (red line) and the SOFTNSM controller (magenta line) from Figures 4–7, it is observed that the overshoot of the proposed RNFTTSM controller is smaller than the SOFTNSM controller, and the convergence rate of RNFTTSM controller is also faster than the SOFNTSMC. By contrasting the response curves under the RNFTTSM controller (red line) and the NFTTSM controller in five different cases of initial states $x(0)$, we can find that the settling time of the proposed RNFTTSMC and the proposed NFTTSMC controller is much the same. This is because the two controllers have the same basic control structure with identical parameters. However, the response curves of angle and angular velocity tracking of PRP under NFTTSM controller have a fluctuation after the system reaching a plateau. This phenomenon shows that RNFTTSM controller has a stronger robustness than NFTTSM, due to the TDDO module imported in RNFTTSM estimating the unknow lumped uncertainty.

2) Fixed time convergence of NFTTSM controller.

Based on the results in Theorem 1 and Theorem 2, the upper bound of the convergence time during reaching phase and sliding mode phase can be calculated by NFTTSM controller

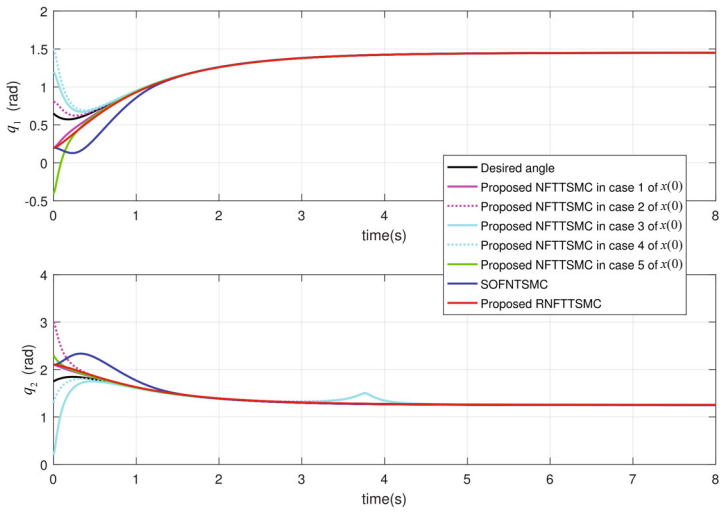

Figure 4 Angle tracking trajectory of ARP and PRP in APDL-SM under three controllers

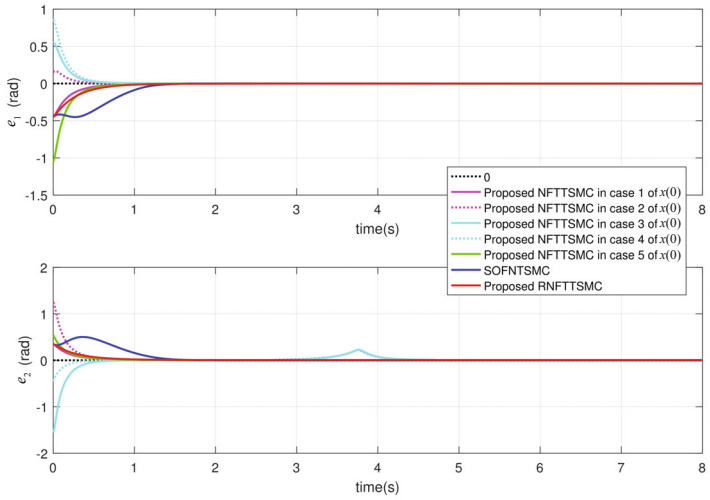

Figure 5 Angle tracking errors trajectory of ARP and PRP in APDL-SM under three controllers

parameters as $t_r \leq T_r = \frac{n}{m-n}{k_1}^{-1} + \frac{q}{q-p}{k_2}^{-1} = 3.75$ s and $t_s \leq T_s = \beta(-1) = 0.125$ s. As a consequence, the total setting time t_c can be estimated as $t_c \leq T_c = T_r + T_s = 3.875$ s. From the curves of five different initial states under NFTTSMC in Figures 4 and 5, it is observed that the proposed NFTTSM controller has fast global convergence speed and the tracking errors decrease to zero promptly. The convergence time under the proposed NFTTSM controller is smaller than 1.5 s, which is much less than the calculated upper bound value before. Therefore, the settling time is independent to the initial states and designable by human, which is satisfied the property of fixed-time convergence. In Figures 6 and 7, the angular velocity and its tracking error trajectory are showed. The results prove the same property of fixed-time convergence for velocity tracking error.

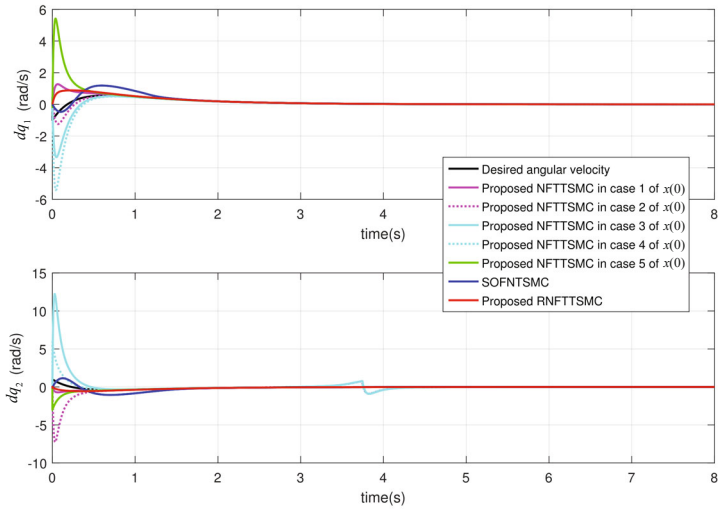

Figure 6 Angular velocity tracking trajectory of ARP and PRP in APDL-SM under three controllers

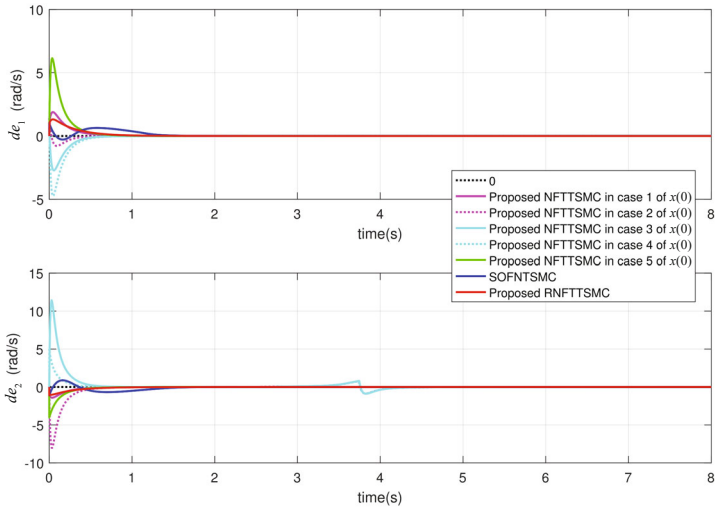

Figure 7 Angular velocity tracking errors trajectory of ARP and PRP in APDL-SM under three controllers

3) One parameter determines the upper bound of settling time on FTTSS.

Considering that the convergence time of sliding mode phase is difficult to be observed intuitively in the whole tracking process, an extra easy numerical simulation on sliding mode phase is constructed to verify that the constant upper bound of settling time is designed by only one parameter. Sliding mode phase is from the beginning of $\sigma = 0$ to the moment that the states settle to the origin of system. Therefore, on the basis of Theorem 1, assign the parameter β in FTTSS with $\mathrm{diag}(2, 4)$. The initial states of positon tracking error on sliding surface are set as $e_1(0) = [3, -1]^{\mathrm{T}}$. The results are shown in Figure 8(a). It can be observed that the convergence time for position tracking error of azimuth angle e_{11} and pitch angle e_{12} is less than $\beta_1^{-1} = 0.5$ s and $\beta_2^{-1} = 0.25$ s, respectively. Consequently, it verified that the convergence time of sliding mode phase has the upper bound β^{-1}. When set $\beta = \mathrm{diag}(5, 8)$, the states curves are shown in Figure 8(b). Theorem 1 can be verified agian. As a consequence, it is clear that the convergence time of the position tracking error on sliding mode phase can be modified optionally by changing the parameter β of our proposed FTTSS.

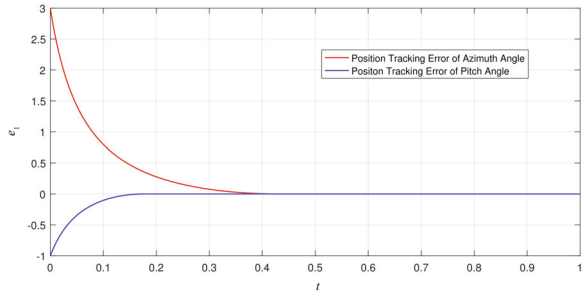

(a) when $\beta = \mathrm{diag}(2, 4)$

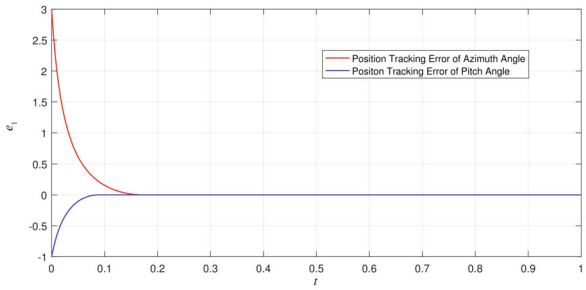

(b) when $\beta = \mathrm{diag}(5, 8)$

Figure 8 Convergence time of sliding mode phase

6 Conclusion

To ensure a high-precision trajectory tracking control of APDL-SM under model uncertainty and lumped external disturbance, a novel RNFTTSM control scheme has been proposed and investigated in this paper. The proposed method mainly consists of three parts: (i) The FTTSS to provide the initial-state-independent convergence and designable convergence time in the sliding mode phase, (ii) the NFTTSM controller with the fixed time reaching law to achieve the fixed-time stability and a settling time estimate for the reaching phase, and (iii) the TDDO part to compensate the impact of model uncertainty and external disturbance on tracking performance and to improve the robustness of the tracking system. The stability of the closed-loop control system is analyzed by using Lyapunov method. Finally, the validity and superiorities of our proposed FTTSS, NFTTSM, and RNFTTSM control scheme are verified through simulation experiments. Although the proposed RNFTTSM control scheme achieves a high-precision trajectory tracking performance under the model uncertainty and lumped external disturbance, there is still a deficiency for us to improve in the future work. The convergence time of both reaching phase and sliding mode phase is designable, but the actual tracking speed is restricted by the upper limit of the torque provided by the actuators. As a consequence, how to balance the designable convergence time with the actuators saturation is an important problem for us to study.

References

[1] Eyring V, Isaksen I S, Berntsen T, et al., Transport impacts on atmosphere and climate: Shipping, *Atmospheric Environment*, 2010, **44**(37): 4735–4771.

[2] Sofiev M, Winebrake J J, and Johansson L, Cleaner fuels for ships provide public health benefits with climate tradeoffs, *Nature Communications*, 2018, **9**(1): 1–12.

[3] Mueller D, Uibel S, and Takemura M, Ships, ports and particulate air pollution — An analysis of recent studies, *Journal of Occupational Medicine and Toxicology*, 2011, **6**(1): 1–6.

[4] IMO, Greenhouse gas study 2014, executive summary and final report, International Maritime Organization, London, 2014.

[5] Smith T, Jalkanen J, and Anderson B, Third IMO greenhouse gas study 2014, *Int. Marit. Organ* 327.

[6] Viana M, Hammingh P, and Colette A, Impact of maritime transport emissions on coastal air quality in Europe, *Atmospheric Environment*, 2014, **90**: 96–105.

[7] Liu H, Fu M, and Jin X, Health and climate impacts of ocean-going vessels in East Asia, *Nature Climate Change*, 2016, **6**(11): 1037–1041.

[8] Liang H, Liu G, and Zhang H, Neural-network-based event-triggered adaptive control of nonaffine nonlinear multiagent systems with dynamic uncertainties, *IEEE Transactions on Neural Networks and Learning Systems*, 2021, **32**(5): 2239–2250.

[9] Zhou Q, Chen G, and Lu R, Disturbance-observer-based event-triggered control for multi-agent systems with input saturation, *Scientia Sinica Informationis*, 2019, **49**(11): 1502–1516.

[10] Zhou Q, Li H, and Shi P, Decentralized adaptive fuzzy tracking control for robot finger dynamics, *IEEE Transactions on Fuzzy Systems*, 2014, **23**(3): 501–510.

[11] Nohooji H R, Constrained neural adaptive pid control for robot manipulators, *Journal of the Franklin Institute*, 2020, **357**(7): 3907–3923.

[12] Han S I and Lee J M, Fuzzy echo state neural networks and funnel dynamic surface control for prescribed performance of a nonlinear dynamic system, *IEEE Transactions on Industrial Electronics*, 2013, **61**(2): 1099–1112.

[13] Kumar C R, Sudha K R, and Pushpalatha D V, Design of prisoner's dilemma based fuzzy logic computed torque controller with Lyapunov synthesis linguistic model for puma-560 robot manipulator, *Journal of Intelligent & Fuzzy Systems*, 2016, **31**(1): 345–355.

[14] Zaare S and Soltanpour M R, Continuous fuzzy nonsingular terminal sliding mode control of flexible joints robot manipulators based on nonlinear finite time observer in the presence of matched and mismatched uncertainties, *Journal of the Franklin Institute*, 2020, **357**(11): 6539–6570.

[15] Capisani L M and Ferrara A, Trajectory planning and second-order sliding mode motion/interaction control for robot manipulators in unknown environments, *IEEE Transactions on Industrial Electronics*, 2011, **59**(8): 3189–3198.

[16] Xiao B, Yin S, and Kaynak O, Tracking control of robotic manipulators with uncertain kinematics and dynamics, *IEEE Transactions on Industrial Electronics*, 2016, **63**(10): 6439–6449.

[17] Chen Q, Yu L, and Nan Y, Finite-time tracking control for motor servo systems with unknown dead-zones, *Journal of Systems Science & Complexity*, 2013, **26**(6): 940–956.

[18] Wang Y, Wang X, Zhao S, et al., Vector field based sliding mode control of curved path following for miniature unmanned aerial vehicles in winds, *Journal of Systems Science & Complexity*, 2018, **31**(1): 302–324.

[19] Sun W and Wu Y, Modeling and finite-time tracking control for mobile manipulators with affine and holonomic constraints, *Journal of Systems Science & Complexity*, 2016, **29**(3): 589–601.

[20] Wang J, Luo X, Li X, et al., Sliding mode formation control of nonlinear multi-agent systems with local lipschitz continuous dynamics, *Journal of Systems Science & Complexity*, 2019, **32**(3): 759–777.

[21] Liu L P, Fu Z M, and Song X N, An adaptive sliding mode control of delta operator systems with input nonlinearity containing unknown slope parameters, *Journal of Systems Science &*

Complexity, 2017, **30**(3): 535–549.

[22] Gan M, Qiao Z, and Li Y, Sliding mode control with perturbation estimation and hysteresis compensator based on bouc-wen model in tackling fast-varying sinusoidal position control of a piezoelectric actuator, *Journal of Systems Science & Complexity*, 2016, **29**(2): 367–381.

[23] Chen J, Tian Y, Li P, et al., Sliding-mode-control based robust guidance algorithm using only line-of-sight rate measurement, *Journal of Systems Science & Complexity*, 2016, **29**(6): 1485–1504.

[24] Chen Q, Tao L, and Nan Y, Full-order sliding mode control for high-order nonlinear system based on extended state observer, *Journal of Systems Science & Complexity*, 2016, **29**(4): 978–990.

[25] Man Z H, Paplinski A P, and Wu H R, A robust mimo terminal sliding mode control scheme for rigid robotic manipulators, *IEEE transactions on Automatic Control*, 1994, **39**(12): 2464–2469.

[26] Mei K, Ding S, Yang X, et al., Second-order sliding mode controller design with a larger domain of attraction, *Journal of Systems Science & Complexity*, 2020, **33**(1): 61–73.

[27] Guo Y, Yu L, and Xu J, Robust finite-time trajectory tracking control of wheeled mobile robots with parametric uncertainties and disturbances, *Journal of Systems Science & Complexity*, 2019, **32**(5): 1358–1374.

[28] Zak M, Terminal attractors for addressable memory in neural networks, *Physics Letters A*, 1988, **133**(1–2): 18–22.

[29] Zak M, Terminal attractors in neural networks, *Neural Networks*, 1989, **2**(4): 259–274.

[30] Venkataraman S and Gulati S, Control of nonlinear systems using terminal sliding modes, *Journal of Dynamic Systems Measurement and Control*, 1992, **115**(3): 891–893.

[31] Yu X H and Man Z H, Fast terminal sliding-mode control design for nonlinear dynamical systems, *IEEE Transactions on Circuits and Systems I: Fundamental Theory and Applications*, 2002, **49**(2): 261–264.

[32] Xu S S D, Chen C C, and Wu Z L, Study of nonsingular fast terminal sliding-mode fault-tolerant control, *IEEE Transactions on Industrial Electronics*, 2015, **62**(6): 3906–3913.

[33] Zheng J, Wang H, Man Z, et al., Robust motion control of a linear motor positioner using fast nonsingular terminal sliding mode, *IEEE/ASME Transactions on Mechatronics*, 2014, **20**(4): 1743–1752.

[34] Polyakov A, Nonlinear feedback design for fixed-time stabilization of linear control systems, *IEEE Transactions on Automatic Control*, 2011, **57**(8): 2106–2110.

[35] Wang N, Zhang T, Yi Y, et al., Adaptive control of output feedback nonlinear systems with unmodeled dynamics and output constraint, *Journal of the Franklin Institute*, 2017, **354**(13): 5176–5200.

[36] Chen Y H and Zhang X, Adaptive robust approximate constraint-following control for mechanical systems, *Journal of the Franklin Institute*, 2010, **347**(1): 69–86.

[37] Vo A T, Nguyen N H A, and Pham D D, Integral sliding mode control for trajectory tracking control of robotic manipulators using an adaptive twisting algorithm, *Journal of Science and Technology: Issue on Information and Communications Technology*, 2019, **17**(12): 42–47.

[38] Cho G R, Chang P H, Park S H, et al., Robust tracking under nonlinear friction using time-delay control with internal model, *IEEE Transactions on Control Systems Technology*, 2009, **17**(6): 1406–1414.

[39] Jin M, Jin Y, Chang P H, et al., High-accuracy tracking control of robot manipulators using time delay estimation and terminal sliding mode, *International Journal of Advanced Robotic Systems*,

2011, **8**(4): 65–78.

[40] Youcef-Toumi K and Ito O, A time delay controller for systems with unknown dynamics, *IEEE American Control Conference*, 1988, 904–913.

[41] Jin M, Lee J, Chang P H, et al., Practical nonsingular terminal sliding-mode control of robot manipulators for high-accuracy tracking control, *IEEE Transactions on Industrial Electronics*, 2009, **56**(9): 3593–3601.

[42] Chang P H and Jeong J W, Enhanced operational space formulation for multiple tasks by using time-delay estimation, *IEEE Transactions on Robotics*, 2012, **28**(4): 773–786.

[43] Van M, Ge S S, and Ren H, Finite time fault tolerant control for robot manipulators using time delay estimation and continuous nonsingular fast terminal sliding mode control, *IEEE Transactions on Cybernetics*, 2016, **47**(7): 1681–1693.

[44] Brahmi B, Saad M, Rahman M H, et al., Adaptive force and position control based on quasi-time delay estimation of exoskeleton robot for rehabilitation, *IEEE Transactions on Control Systems Technology*, 2019, **28**(6): 2152–2163.

[45] Siciliano B, Sciavicco L, Villani L, et al., *Robotics: Modelling, Planning and Control*, Springer Science & Business Media, Berlin, 2010.

[46] Brahmi B, Saad M, Ochoa-Luna C, et al., Adaptive tracking control of an exoskeleton robot with uncertain dynamics based on estimated time-delay control, *IEEE/ASME Transactions on Mechatronics*, 2018, **23**(2): 575–585.

[47] Ni J, Liu L, Liu C, et al., Fast fixed-time nonsingular terminal sliding mode control and its application to chaos suppression in power system, *IEEE Transactions on Circuits and Systems II: Express Briefs*, 2016, **64**(2): 151–155.

[48] Zuo Z, Non-singular fixed-time terminal sliding mode control of non-linear systems, *IET Control Theory & Applications*, 2014, **9**(4): 545–552.

[49] Chang P H and Jeong J W, Enhanced operational space formulation for multiple tasks by using time-delay estimation, *IEEE Transactions on Robotics*, 2012, **28**(4): 773–786.

[50] Roy S, Kar I N, Lee J, et al., Adaptive-robust time-delay control for a class of uncertain Euler-Lagrange systems, *IEEE Transactions on Industrial Electronics*, 2017, **64**(9): 7109–7119.

[51] Baek J, Kwon W, and Kim B, A widely adaptive time-delayed control and its application to robot manipulators, *IEEE Transactions on Industrial Electronics*, 2018, **66**(7): 5332–5342.

[52] Yi S and Zhai J, Adaptive second-order fast nonsingular terminal sliding mode control for robotic manipulators, *ISA Transactions*, 2019, **90**: 41–51.

[53] Wang Z and Shan J, Fixed-time consensus for uncertain multi-agent systems with actuator faults, *Journal of the Franklin Institute*, 2020, **357**(2): 1199–1220.

[54] Huo B, Xia Y, Lu K, et al., Adaptive fuzzy finite-time fault-tolerant attitude control of rigid spacecraft, *Journal of the Franklin Institute*, 2015, **352**(10): 4225–4246.